

Modeling and adaptive neuro-fuzzy inference system control of quarter electric vehicle

Rachida Baz¹, Khalid El Majdoub², Fouad Giri³, Ossama Ammari¹

¹Laboratory of Materials, Energy and Control System, Department of Electric Engineering, FST Mohammedia, University Hassan II, Mohammedia, Morocco

²ENSEM, University Hassan II, Casablanca, Morocco

³University of Caen Normandie, ESIX Normandie, Caen, France

Article Info

Article history:

Received Nov 27, 2023

Revised Jan 11, 2024

Accepted Feb 16, 2024

Keywords:

ANFIS controller

BLDC motor

Electric vehicle

Fuzzy controller

PACEJKA tire model

PID controller

ABSTRACT

Electric vehicles (EVs) have gained importance in recent years, prompting the development of several control systems to improve their efficiency and performance. In this work, a quarter electric vehicle (QEV) was controlled using a conventional proportional integral derivative (PID) and fuzzy controller to examine and compare with the response of the adaptive neuro-fuzzy inference system (ANFIS) controller. The response of the ANFIS controller was evaluated using MATLAB/Simulink according to different parameters and compared with those of other controllers. In addition, the simulation was based on different driving conditions such as the acceleration and deceleration modes and the type of road: wet and dry. The simulations were carried out on a longitudinal electric vehicle model based on a brushless DC motor, including the Pacejka tire model. The results showed that the ANFIS controller outperformed the PID and fuzzy logic controllers, providing superior dynamic responsiveness and stability when the ANFIS controller smoothly followed the input speed and the longitudinal slip value reached 3%.

This is an open access article under the [CC BY-SA](#) license.



Corresponding Author:

Rachida Baz

Laboratory of Materials, Energy and Control System, Department of Electric Engineering

FST Mohammedia, University Hassan II

Mohammedia, Morocco

Email: rachida.baz@gmail.com

1. INTRODUCTION

The new generation of transportation promotes green technology that protects the environment from harmful CO₂ and gas emissions by referring to Industry 4.0 [1], which supports the orientation towards electric vehicles (EVs) for their various advantages, namely zero emissions and low maintenance costs [2]. EVs are driven by electric motors and powered by lithium-ion batteries [3]. Instead of combustion engines which are less efficient by 50%, EVs can convert up to 90% of the energy consumed, thus providing instantaneous couple with various charges. In addition, EVs can restore energy through braking [4]. On the other hand, thanks to the lack of a gearbox and moving parts, EVs are characterized by a reduced size compared to those powered by the combustion engine [5].

In terms of electric car motorization, literature has highlighted various types of motors, such as the DC motor which was among the first motors used for its high torque and low speed, however, its disadvantages have limited its use namely: brushes and commutator require replacement due to the effect of mechanical aging associated with friction, also the motor requires high maintenance [6]. The other category is a brushless DC motor (BLDC), it is used in various fields and applications due to its low maintenance,

good manageability, high efficiency, and small size [7], [8]. It is built with a stator wound with wires to offer an adjustable flux density and a permanent magnet rotor with differential pole counts [9]. The stator coils, which are controlled by Hall sensors and powered by DC voltage, offer great efficiency and power density with less noise. By using sensorless predictive design, this design can be further enhanced by reducing metal losses, and ripple [10]. A BLDC motor drive is highly complex, requiring modeling, control scheme selection, simulation, and parameterization, among other things [11]. To ensure driver safety and proper vehicle handling, control modules like the body control unit are getting increasingly sophisticated and smart. The simplicity of control is important to note among the other benefits provided by EVs [12].

The categories of available controllers are conventional namely proportional integral derivative (PID) and adaptive among others fuzzy and adaptive neuro-fuzzy inference system (ANFIS) controllers [13], the PID control parameter tuning is very challenging and robustness is limited [14]. A fixed controller does not function properly at all speeds and an adaptive controller is preferable because of the load non-linearity and evolving machine requirements at different speed ranges [15]. Fuzzy control can take appropriate control parameters and do calculations more quickly than PID controller, which has difficulty taking the proper characteristics [16]. The benefits of both fuzzy and neuro-system control can be found in a neuro-fuzzy adaptive control system [17].

In this study, speed controller performances are analyzed and compared for conventional controller PID and adaptive fuzzy PID controller, as well as for an ANFIS controller. A quarter electric vehicle (QEV) drives the BLDC motor during the simulation of the comparison using MATLAB/Simulink. The following objectives can be used to express this paper's goals: to offer an exhaustive and effective method for designing a controller based on adaptive fuzzy PID (AFPID) and ANFIS.

This paper is organized into three primary sections. Initially, it begins with a broad introduction, outlining the primary software employed in this study, which is MATLAB/Simulink. It also provides an overview of BLDC motors and fuzzy logic. The second section delves into the methodologies utilized for this simulation, which encompass the mathematical modeling of the BLDC motor, the quarter electric vehicle, and the design of the fuzzy controller. In the final section, we explore the simulation and its outcomes, concluding with a summary of our findings.

2. METHODS

2.1. BLDC motor and fuzzy logic

Brushless direct current denoted as BLDC motor is utilized in versatile industrial applications such as aerospace, and electric cars. thanks to its several advantages such as high efficiency and not causing sparks. This motor's functioning is based on electronic commutation, and a sequence of commutation to feed the stator. To detect the right position of the rotor, the BLDC motor uses a sensorless technique, or it is equipped with three hall effect sensors (Ha, Hb, and Hc), which are placed close to the stator [18]. But, still, this motor suffers from some defaults as slow response to the set point and its speed is not constant in different loads Thus, a performant controller has to be established to control the system and improve its performance [19].

Fuzzy logic is an evolution of classical logic systems that delivers a basis of notions appropriate to the particular task of constructing knowledge-based representations in a context of uncertainty and imprecision. The representation of meaning in fuzzy logic is based on the semantics of test scores. In this method, a proposition is perceived as a system of flexible constraints. Reasoning is seen as the propagation of elastic constraints [20], [21]. Understanding BLDC motor drawbacks and the role of fuzzy logic unveils opportunities to revolutionize control strategies, enhancing motor response and overall efficiency.

2.2. Brushless DC motor: mathematical modeling

2.2.1. Design of BLDC motor

The BLDC motor drive's basic drive diagram is illustrated in Figure 1. The front end of the inverter receives DC power input, and the motor terminals are connected to the inverter output. Each phase of the motor is represented by a series-coupled inductance, resistance, and a voltage source with a back electromotive force (EMF). The structure necessary for assessing the BLDC motor's operating principle during the conduction mode.

In a BLDC motor, the stator is made up of three-phase windings, while the rotor is constructed of permanent magnets implanted therein, Hall effect sensors as shown in Figure 2, which serve to electronically shift the rotor, detect its exact position by detecting whether the rotor magnetic poles are N or S as shown in Figure 2(a), and send a high or low signal accordingly. The commutation sequence can be figured out from the combination of these three signals from the Hall sensors. As a result, sequentially activating three-phase stator coils causes the motor shaft to rotate. Back EMF occurs as a result of rotation, and its shape is trapezoidal, as seen in Figure 2(b). Refer to for a summary of machine functionality [22].

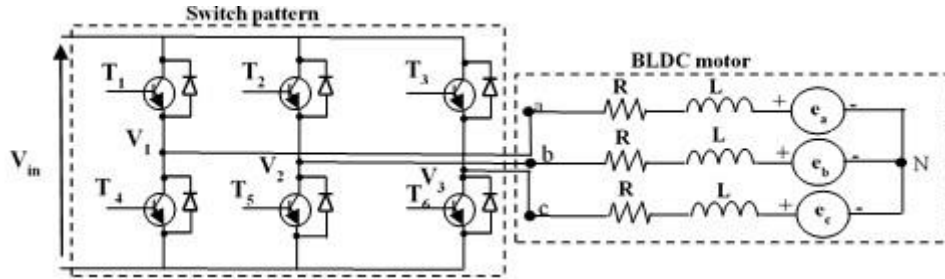


Figure 1. Diagram of the electrical circuit of the BLDC motor associated with the inverter

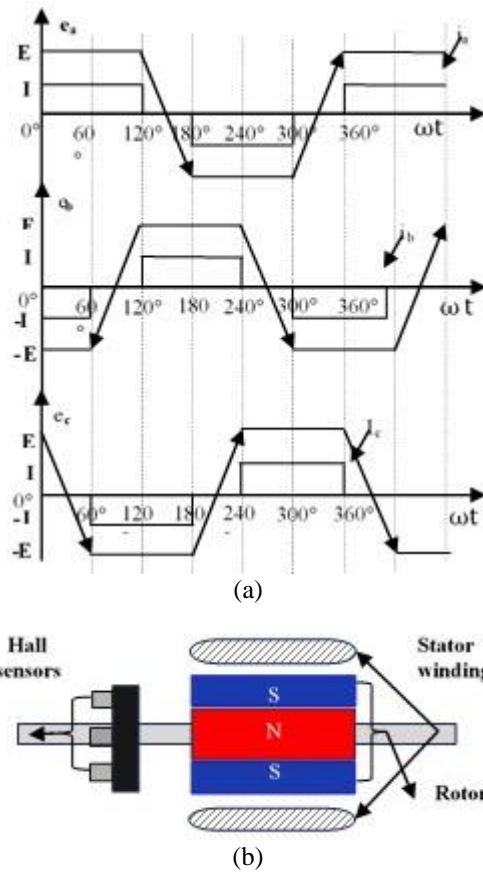


Figure 2. BLDC motor components and current and voltage behavior across three phases (a) transverse section of a BLDC motor revealing stator poles, rotor, and hall effect sensors and (b) currents and EMF waveforms of three phases A, B, and C of BLDC motor

A few assumptions were made in the modeling phase of the BLDC motor, such as negligible losses, the value of inductances being constant, equal resistances in all phases, and EMFs of phases a, b, and c have the same magnitudes. In (1) shows the three-phase voltages of the motor. In (2) and (3) describe the electromagnetic and mechanical torque [9].

$$\begin{bmatrix} v_a \\ v_b \\ v_c \end{bmatrix} = \begin{bmatrix} R & 0 & 0 \\ 0 & R & 0 \\ 0 & 0 & R \end{bmatrix} \begin{bmatrix} i_a \\ i_b \\ i_c \end{bmatrix} + \begin{bmatrix} L & M & M \\ M & L & M \\ M & M & L \end{bmatrix} \frac{d}{dt} \begin{bmatrix} i_a \\ i_b \\ i_c \end{bmatrix} + \begin{bmatrix} e_a \\ e_b \\ e_c \end{bmatrix} \tag{1}$$

$$T_e = \frac{i_a \cdot e_a + i_b \cdot e_b + i_c \cdot e_c}{\omega} \tag{2}$$

$$T_e = J_r \dot{\omega} + F\omega + T_L \tag{3}$$

Where:

v_i : phase voltages, (i refers to the three phases' phases)

i_i : phase currents

e_i : back EMF

R : the stator resistance

L : the inductance

M : the mutual inductance

ω : the rotor speed

J_r : rotor inertia

F : friction constant

T : load torque

2.2.2. Mathematical representation of trapezoidal EMF

The generation of EMF is strongly dependent on the position of the rotor detected by Hall sensors as listed in Table 1, which is determined by the speed [23], as shown in (4). The shape of the back-EMF is given by $f_i(\theta)$. It is calculated based on (5) in a single period.

$$\begin{bmatrix} e_a \\ e_b \\ e_c \end{bmatrix} = E \begin{bmatrix} f_a(\theta) \\ f_b(\theta) \\ f_c(\theta) \end{bmatrix}, E = K_e \omega_r \tag{4}$$

K_e : the back-EMF constant

θ : the position of the rotor

ω_r : the angular velocity of the rotor

Table 1. The sequence of the hall effect during one period

| Rotor location | Electrical degree | Hall signal (ABC) | Sample phase | Sign relationship with the given value | Open phase | Turn off phase |
|----------------|-------------------|-------------------|--------------|----------------------------------------|------------|----------------|
| 1 | 0-60 | 101 | B | + | A | C |
| 2 | 60-120 | 100 | A | - | C | B |
| 3 | 120-180 | 110 | C | + | B | A |
| 4 | 180-240 | 010 | B | - | A | C |
| 5 | 240-300 | 011 | A | + | C | B |
| 6 | 300-360 | 001 | C | - | B | A |

$$f_a(\theta) = \begin{cases} \frac{6}{\pi} & (0 < \theta \leq \frac{\pi}{6}) \\ 1 & (\frac{\pi}{6} < \theta \leq \frac{5\pi}{6}) \\ -\left(\frac{6}{\pi}\right)\theta + 6 & (\frac{5\pi}{6} < \theta \leq \frac{7\pi}{6}) \\ -1 & (\frac{7\pi}{6} < \theta \leq \frac{11\pi}{6}) \\ \left(\frac{6}{\pi}\right)\theta - 12 & (\frac{11\pi}{6} < \theta \leq 2\pi) \end{cases} \tag{5}$$

2.3. Modeling of the quarter electric vehicle

The system's schematic representation can be found in Figure 3, featuring a composition of the Pacejka tire model and a BLDC in-wheel motor. To gain insight into the Pacejka model's properties, they are presented in Table 2. In (8) encapsulates the magic formula or Pacejka model, forming a critical element within the system. Additionally (6) and (7) represent the system's equations, delineating its behavior and dynamics. Notably, for this analysis, we omit consideration of longitudinal and lateral forces, focusing exclusively on specific aspects of the system's performance. the QEV representation in interaction with the road illustrated in Figure 3 is presented in this paper. The studied system is supposed to track a linear path. Adopting the Newton's first law, the (6) is obtained.

$$m_v \dot{v}_x = F_x \tag{6}$$

where m_v is the masse of the QEV (kg), \dot{v}_x represents the velocity of the system (m/s) and the F_x is longitudinal force depending on the interaction between the tire and the road surface acting on the wheel (N).

Newton's second principle is used to calculate T_e , the equation will be set as (7). Tire modeling is difficult due to its complicated behavior, but it is critical for vehicle dynamics. Based on empirical data, the Pacejka tire model defines the adhesion coefficient (μ) as an expression of longitudinal slip (σ) as illustrated in (8) [24].

$$T_e = J\dot{\Omega}_\omega + F_x r_{eff} + M_{rr} \tag{7}$$

Where T_e is the electromagnetic torque produced (Nm), the moment of inertia of the driving wheel is defined by j (kg/m^2), Ω_ω is the rotational velocity of the driving wheel (rads^{-1}), r_{eff} is the effective radius (m), and F_x is the traction or braking force (N).

$$\mu(\sigma) = D \sin(C \tan^{-1}(B\sigma - E (B\sigma - \tan(B\sigma)))) \tag{8}$$

Where the parameters B is the stiffness factor, D is the shape factor, C is the peak value and E is the curvature factor [25]. The values of B , C , D and E for various types of asphalt road conditions are provided in Table 2.

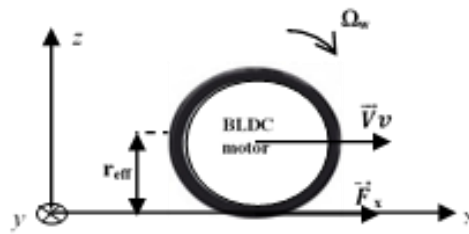


Figure 3. Model of QEV incorporating BLDC motor on a road, depicting force F_x , vehicle speed, and effective radius

Table 2. Pacejka equation coefficients adapted to road conditions

| | Dry | Wet | Snow | Ice |
|---|------|------|------|-----|
| B | 10 | 12 | 5 | 4 |
| C | 1.9 | 2.3 | 2 | 2 |
| D | 1 | 0.82 | 0.3 | 0.1 |
| E | 0.97 | 1 | 0.1 | 1 |

As depicted in (9), the longitudinal force F_x is determined by the coefficient of adhesion and the normal force F_v exerted on the wheel. In (10) provides a general expression for the slip ratio, which depends on both wheel linear speed and vehicle speed. In (11) and (12) are derived specifically for acceleration and deceleration modes, respectively, and provide an overview of these distinct operating conditions.

$$\mu = \frac{F_x}{F_v} \tag{9}$$

$$\sigma = \frac{r\omega - v_x}{\max(v_x, r\omega)} \tag{10}$$

$$\sigma = 1 - \frac{v_x}{r_{eff} \omega} \tag{11}$$

$$\sigma = \frac{r_{eff} \omega}{v_x} - 1 \tag{12}$$

2.4. The conception of the speed controller

The design of the controller is based on fuzzy logic and the neural network represented in Figure 4 forming the ANFIS controller. The main purpose of fuzzy logic is to make decisions in the absence of reliable, accurate, or complete data [26]. It was initiated based on models or knowledge using fuzzy rules. The result of fuzzy inference processes is the transformation of ordinary input data into understandable and interpretable output data through operations of fuzzification and defuzzification, and fuzzy rules, membership functions (MF) as illustrated in Figure 4(a) [27].

The fuzzy inference system (FIS) is subdivided mainly into two categories-Mamdani and Takagi-Sugeno. Nevertheless, the fundamental core of a FIS lies in the establishment of the rule base, which presents two major obstacles: the establishment of a rule base requires expert knowledge of the field of study, and the refinement of the MF base is a key element of the process to reduce the output error. The present study utilizes an ANFIS to attain the identification and fine-tuning of a FIS [28]. The global structure of the ANFIS shares the same elements as the FIS, except for the neural network component which Includes numerous nodes that resemble human neurons [29]. it is a multi-layer controller It resembles a FIS but incorporates back-propagation to reduce errors. In ANFIS, fuzzy if-then rules of the Takagi and Sugeno type 2 are employed for making inferences. This rule base is part of the ANFIS control structure, which comprises five interconnected network layers and encompasses: fuzzification, knowledge base, neural network, and defuzzification [30].

During the evaluation, data was generated and fed into the neuro-fuzzy designer. The FIS was constructed using a grid-based partition and featured two input variables: U and V, with a single output denoted by Y, which is specified by the function $Y=f(U, V)$. Here, U represents the error input (denoted by "e"), and V stands for the rate of change of the error, denoted by "de". The FIS data was trained using a hybrid optimization technique with zero error tolerance and 100 epochs, and with the data training the FIS, controller reached $2.66844 \cdot 10^{-8}$. Considering these factors, Figure 4(b) illustrates the structure of the five-layer ANFIS.

The main principle of ANFIS with two inputs, U and V, and a single output Y, might be expressed as shown below:

Rule 1: If U is A_1 and V is B_1 , then $Y_1=p_1U+q_1V+r_1$.

Rule 2: If U is A_2 and V is B_2 , then $Y_2=p_2U+q_2V+r_2$.

Here, A_i and B_i denote the parameters of the fuzzy sets for each input in the precondition part, while p_i , q_i , and r_i denote the linear parameters in the consequent part. The ANFIS structure consists of five layers and is used for two inputs and one output.

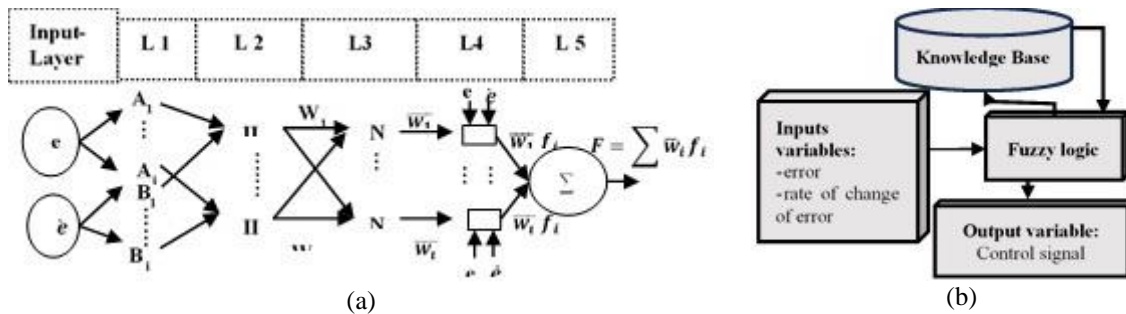


Figure 4. General architecture of the ANFIS controller (a) the structure of five layers ANFIS and the layer of the inputs and (b) input-output mapping

Fuzzifying layer 1: the expression for each adaptive node (i) within this layer, is outlined as (13). In this context, A_i (or B_i) corresponds to a linguistic label associated with this particular node, while e (or \dot{e}) signifies the input for node i. The input variables are commonly characterized using the Gaussian membership function as defined in (14), with c as the center, and σ denoting the width of the membership function.

$$\begin{aligned} L_{1,i} &= \mu_{A_i}(e) \text{ for } i = 1,2, \dots, j \\ L_{1,i} &= \mu_{B_i}(\dot{e}) \text{ for } i = 1,2, \dots, j \end{aligned} \tag{13}$$

$$f(x; \sigma, c) = e^{-\frac{(x-c)^2}{2\sigma^2}} \tag{14}$$

Implication layer 2: its output is the cumulative total of all acquired signals. As illustrated in (15), the formula for the output node of this layer is given by (15). The firing strength of a rule is indicated by each node output.

$$L_{2,i} = w_i = \mu_{A_i}(e)\mu_{B_i}(\dot{e}) \text{ for } i = 1,2, \dots, j^2 \tag{15}$$

Normalizing layer 3: this layer exclusively comprises fixed nodes, each labeled as N. Each of these nodes, denoted as the i^{th} node, calculates the firing strength of the i^{th} rule relative to the total firing strength of all rules. According to the node in (16) for this layer.

$$L_{3,i} = \bar{W} = \frac{w_i}{\sum_{i=1}^{j^2} w_i} \tag{16}$$

Defuzzifying layer 4: in this layer, each node labeled as i is adaptive, and its function is defined by (17). In this context, \bar{W} represents the normalized firing strength of layer 3, and (p_i, q_i, r_i) denotes the parameter set for this particular node. These settings in this layer are referred to as consequential settings, and they are subject to adjustment during the learning process.

$$L_{4,i} = \bar{W}_i f_i = \bar{W}_i (p_i e + q_i \dot{e} + r_i) \tag{17}$$

Combining layer 5: in this layer, there is a single node labeled as ' Σ ' that determines the total output as the sum of all entering signals. As represented in (18), this node's summation is expressed as (18).

$$L_{5,i} = \sum_{i=1}^{j^2} \bar{W}_i f_i = \frac{\sum_{i=1}^{j^2} w_i f_i}{\sum_{i=1}^{j^2} w_i} \tag{18}$$

3. SIMULATION AND DISCUSSION

The QEV system simulation, performed using MATLAB/Simulink as shown in Figure 5, incorporates two crucial factors: the driver's initial speed and the road type. In this study, we assume a constant vehicle speed of 60 km/h. The driver's velocity is represented as a filtered speed input to approximate real-world acceleration and deceleration as shown in Figure 6. The parameters of the BLDC motor are depicted in Table 3, and those of the modeled system QEV in Table 4. Where R , L , and j are the stator resistance, inductance, and rotor inertia respectively. The electric vehicle parameters are m , j , μ_{rr} , r_{eff} , and g which represent, respectively, the mass of QEV, moment of inertia of the driving wheel, coefficient of rolling resistance, wheel radius, and gravity acceleration.

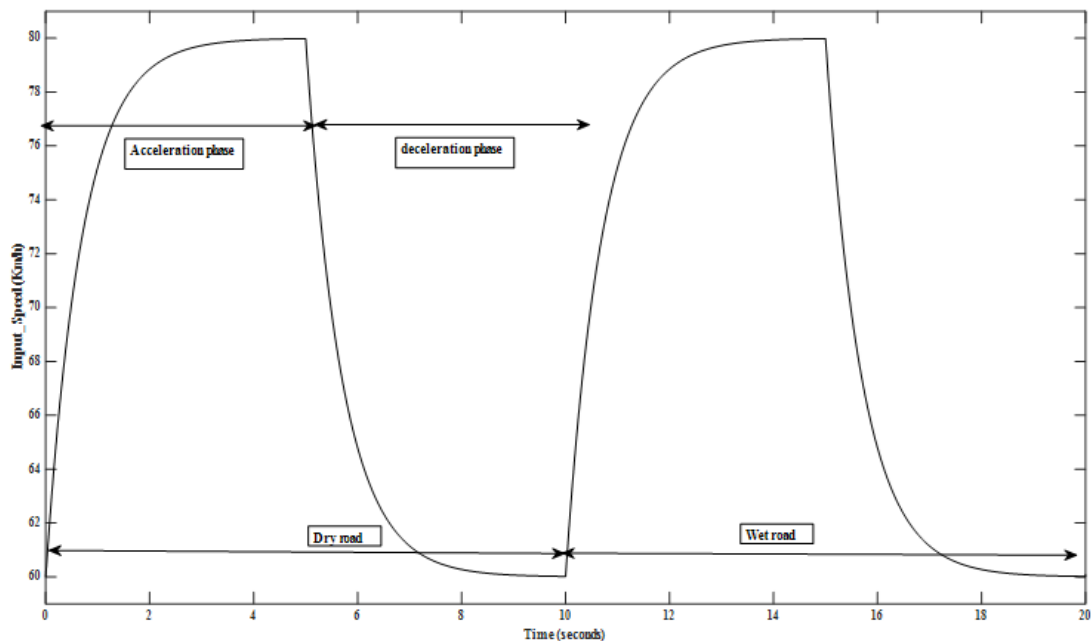


Figure 5. Driver's speed input (acceleration and deceleration) on different types of road (dry and wet)

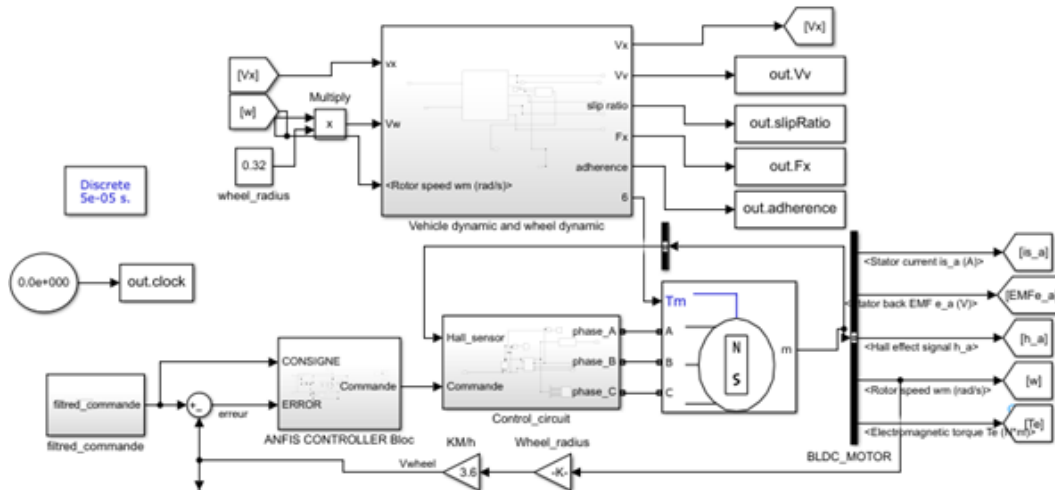


Figure 6. The QEV model simulation on SIMULINK including BLDC motor and PACEJKA tire model

Table 3. BLDC motor parameters

| Symbol | Value |
|------------|------------------------|
| m | 270 kg |
| J | 0.75 kg.m ² |
| μ_{rr} | 0.025 |
| r_{eff} | 0.32 m |
| g | 9.81 m.s ⁻² |

Table 4. System QEV parameters

| Parameters | Value |
|----------------------|---------------------|
| R: stator resistance | 0.2 Ω |
| L: inductance | 8.5 e-4 H |
| j: rotor inertia | 1 kg.m ² |

In the first stage, between 0 s and 10 s, the simulation was run on a dry road, and then on a wet road between 10 s and 20 s, as depicted in Figure 5. Figure 6 shows the speed demanded by the driver, which contains two main phases of acceleration and deceleration during driving on dry and wet roads. The response of the studied controllers: ANFIS, fuzzy controller, and PID are depicted on Figures 7 and 8. Figure 7(a) illustrates the linear wheel speed in phases of acceleration and deceleration, clearly showing that the ANFIS controller smoothly tracks the input speed, while the fuzzy controller and the PID do not reach the speed set by the driver. The vehicle speed delivered by the three controllers is shown in Figure 7(b) which shows the fast response of the ANFIS controller.

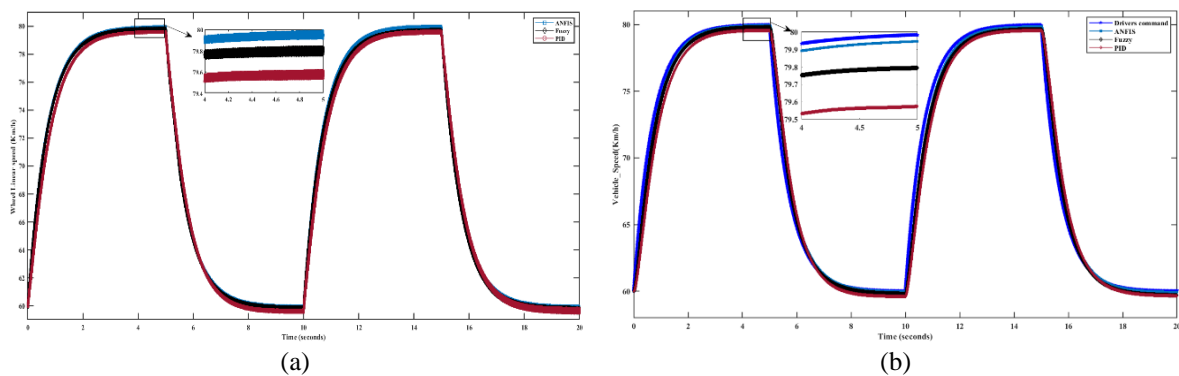


Figure 7. System response of the three controllers (a) linear wheel speed response and (b) controller comparison for vehicle speed during acceleration and deceleration phases on various road types

The longitudinal force F_x in Figure 8(a) is taken into account to compare the controllers' performances. It reaches 1535.8 N, 1540 N, and 1320 N for ANFIS, fuzzy, and PID respectively during acceleration, and -1389 N, -1380.78 N, and -1325 N during deceleration on a dry road. ANFIS and the fuzzy controller have close values during the two phases of operation. However, between 5 s and 10 s, the variations of the fuzzy controller are more significant than those provided by the ANFIS controller. Still, the PID has a lower value of longitudinal force than the others, which mainly justifies the fact that it does not reach the required speed. Figure 8(b) presents the longitudinal slip of the vehicle. The ANFIS controller provides the value of the slip ratio by 3% during acceleration compared to the other controllers, and it provides a negative value in deceleration which is -2.61%.

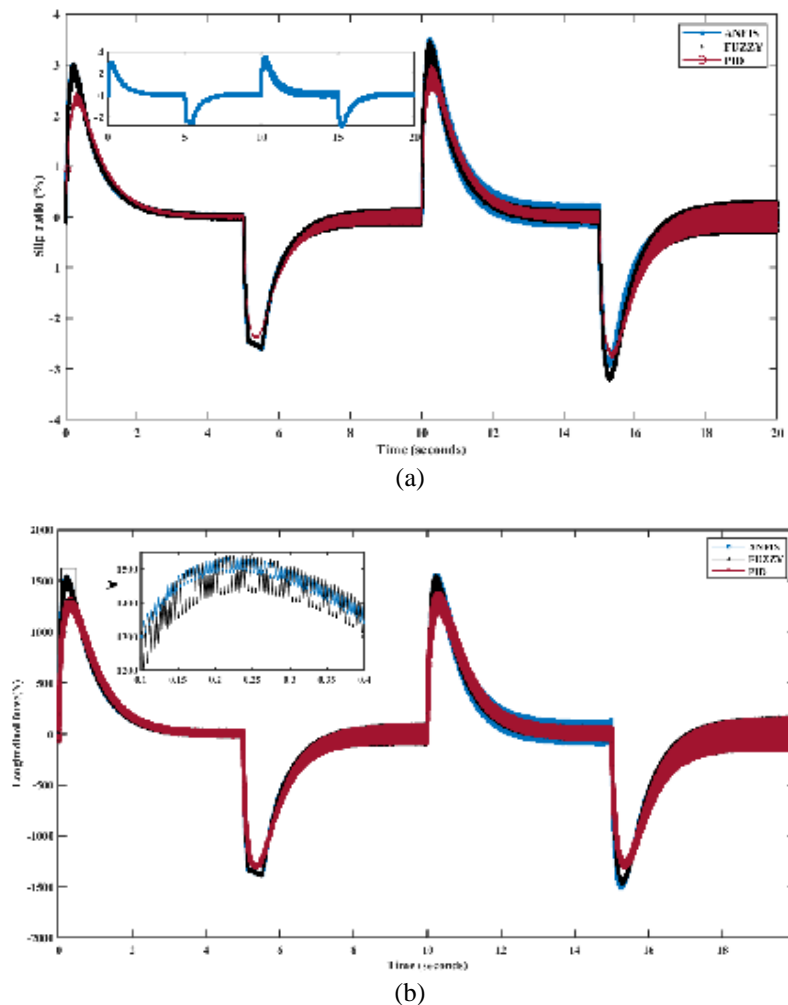


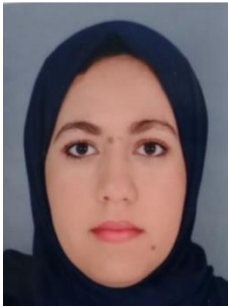
Figure 8. Longitudinal behavior of QEV(a) slip ratio of the QEV resulting from controllers and (b) longitudinal force during acceleration and deceleration on dry and wet road




4. CONCLUSION

This paper carried out an analysis of an electric vehicle quarter model driven by a BLDC motor, including the Pacejka tire model. In addition, the performance of three different system controllers was compared: the adaptive ANFIS controller, the conventional PID controller, and the fuzzy controller. The simulation results demonstrate the superiority of the ANFIS controller in terms of performance and efficiency on different types of roads, namely wet and dry, during acceleration and deceleration. Considering that the vehicle is traveling at 60 km/h on the road, the study firmly establishes that the ANFIS controller consistently outperforms the other studied controllers, offering better control, responsiveness, and adaptability to the dynamic characteristics of the electric vehicle model. This significant performance can be attributed to the ANFIS controller's ability to exploit the advantages of fuzzy logic and neural networks, resulting in a more robust and adaptive control system.




REFERENCES

- [1] P. Bradu *et al.*, "Recent advances in green technology and Industrial Revolution 4.0 for a sustainable future," *Environmental Science and Pollution Research*, vol. 30, no. 60, pp. 124488–124519, Apr. 2022, doi: 10.1007/s11356-022-20024-4.
- [2] J. A. Sanguesa, V. Torres-Sanz, P. Garrido, F. J. Martinez, and J. M. Marquez-Barja, "A review on electric vehicles: technologies and challenges," *Smart Cities*, vol. 4, no. 1, pp. 372–404, Mar. 2021, doi: 10.3390/smartcities4010022.
- [3] S. S. Rangarajan *et al.*, "Lithium-ion batteries—the crux of electric vehicles with opportunities and challenges," *Clean Technologies*, vol. 4, no. 4, pp. 908–930, Sep. 2022, doi: 10.3390/cleantechnol4040056.
- [4] D. Rimpas, S. D. Kaminaris, D. D. Piromalis, G. Vokas, K. G. Arvanitis, and C.-S. Karavas, "Comparative review of motor technologies for electric vehicles powered by a hybrid energy storage system based on multi-criteria analysis," *Energies*, vol. 16, no. 6, p. 2555, Mar. 2023, doi: 10.3390/en16062555.
- [5] F. Alanazi, "Electric vehicles: benefits, challenges, and potential solutions for widespread adaptation," *Applied Sciences*, vol. 13, no. 10, p. 6016, May 2023, doi: 10.3390/app13106016.
- [6] S. Sharma, A. K. Panwar, and M. M. Tripathi, "Storage technologies for electric vehicles," *Journal of Traffic and Transportation Engineering (English Edition)*, vol. 7, no. 3, pp. 340–361, Jun. 2020, doi: 10.1016/j.jtte.2020.04.004.
- [7] L. Yang, J. Zhao, L. Yang, X. Liu, and L. Zhao, "Investigation of a stator-ironless brushless DC motor with non-ideal back-EMF," *IEEE Access*, vol. 7, pp. 28044–28054, 2019, doi: 10.1109/access.2019.2901632.
- [8] D. Mohanraj *et al.*, "A review of BLDC motor: State of art, advanced control techniques, and applications," *IEEE Access*, vol. 10, pp. 54833–54869, 2022, doi: 10.1109/access.2022.3175011.
- [9] R. Baz, K. El Majdoub, F. Giri, and A. Taouni, "Self-tuning fuzzy PID speed controller for quarter electric vehicle driven by In-wheel BLDC motor and Pacejka's tire model," *IFAC-PapersOnLine*, vol. 55, no. 12, pp. 598–603, 2022, doi: 10.1016/j.ifacol.2022.07.377.
- [10] J. C. Gamazo-Real, E. Vázquez-Sánchez, and J. Gómez-Gil, "Position and speed control of brushless DC motors using sensorless techniques and application trends," *Sensors*, vol. 10, no. 7, pp. 6901–6947, Jul. 2010, doi: 10.3390/s100706901.
- [11] G. Shokri and E. Naderi, "Research on simulation and modeling of simple and cost-effective BLDC motor drives," *International Journal of Modelling and Simulation*, vol. 37, no. 1, pp. 15–24, Aug. 2016, doi: 10.1080/02286203.2016.1195665.
- [12] N. Prabhu, R. Thirumalaivasan, and B. Ashok, "Critical review on torque ripple sources and mitigation control strategies of BLDC motors in electric vehicle applications," *IEEE Access*, vol. 11, pp. 115699–115739, 2023, doi: 10.1109/access.2023.3324419.
- [13] B. Rachida, E. M. Khalid, G. Fouad, and A. Ossama, "Implementation and analysis of adaptive neural fuzzy inference system based brushless DC motor," May 2023, doi: 10.1109/iraset57153.2023.10152892.
- [14] S. B. Joseph, E. G. Dada, A. Abidemi, D. O. Oyewola, and B. M. Khammas, "Metaheuristic algorithms for PID controller parameters tuning: review, approaches and open problems," *Heliyon*, vol. 8, no. 5, p. e09399, May 2022, doi: 10.1016/j.heliyon.2022.e09399.
- [15] M. Mahmud, S. M. A. Motakabber, A. H. M. Z. Islam, A. N. Nordin, and S. A. F. Wafa, "Advanced adaptive PID controller for BLDC motor," Jun. 2021, doi: 10.1109/icce50029.2021.9467185.
- [16] A. H. Mohamed, "Comparative study between PID and fuzzy PID controller for speed control of BLDC motor," *International Journal of Engineering Research and*, vol. V7, no. 05, May 2018, doi: 10.17577/ijertv7is050098.
- [17] N. Hooda and M. Malik, "Review on neuro-fuzzy system," *SSRN Electronic Journal*, 2022, doi: 10.2139/ssrn.4033495.
- [18] M. A. Baba, M. Naoui, and M. Cherkaoui, "Fault-tolerant control strategy for hall sensors in BLDC motor drive for electric vehicle applications," *Sustainability*, vol. 15, no. 13, p. 10430, Jul. 2023, doi: 10.3390/su151310430.
- [19] F. Dumitrache, M. Romanca, and G. Pana, "Methods for optimizing BLDC motors performance by using different control schemes," May 2017, doi: 10.1109/optim.2017.7975048.
- [20] J. M. Belman-Flores, D. A. Rodríguez-Valderrama, S. Ledesma, J. J. García-Pabón, D. Hernández, and D. M. Pardo-Cely, "A review on applications of fuzzy logic control for refrigeration systems," *Applied Sciences*, vol. 12, no. 3, p. 1302, Jan. 2022, doi: 10.3390/app12031302.
- [21] O. Castillo and P. Melin, "A review on interval type-2 fuzzy logic applications in intelligent control," *Information Sciences*, vol. 279, pp. 615–631, Sep. 2014, doi: 10.1016/j.ins.2014.04.015.
- [22] C. H. B. Apriboowo, M. Ahmad, and H. Maghfiroh, "Fuzzy logic controller and its application in brushless DC motor (BLDC) in electric vehicle - a review," *Journal of Electrical, Electronic, Information, and Communication Technology*, vol. 3, no. 1, p. 35, Apr. 2021, doi: 10.20961/jeeict.3.1.50651.
- [23] O. Ammari, K. El Majdoub, R. Baz, and A. Taouni, "Longitudinal modelling of electric vehicle driven by a BLDC In-wheel motor based on Pacejka tire model," Jun. 2021, doi: 10.1109/icecce52056.2021.9514238.
- [24] R. B. Kogbara, E. A. Masad, E. Kassem, A. (Tom) Scarpas, and K. Anupam, "A state-of-the-art review of parameters influencing measurement and modeling of skid resistance of asphalt pavements," *Construction and Building Materials*, vol. 114, pp. 602–617, Jul. 2016, doi: 10.1016/j.conbuildmat.2016.04.002.
- [25] E. Bakker, L. Nyborg, and H. B. Pacejka, "Tyre modelling for use in vehicle dynamics studies," Feb. 1987, doi: 10.4271/870421.
- [26] I. Dzitac, F. G. Filip, and M.-J. Manolescu, "Fuzzy logic is not fuzzy: world-renowned computer scientist lotfi A. Zadeh," *International Journal of Computers Communications & Control*, vol. 12, no. 6, p. 748, Dec. 2017, doi: 10.15837/ijccc.2017.6.3111.
- [27] H. -J. Zimmermann, "Fuzzy set theory," *WIREs Computational Statistics*, vol. 2, no. 3, pp. 317–332, May 2010, doi: 10.1002/wics.82.
- [28] A. S. Koshiyama, R. Tanscheit, and M. M. B. R. Vellasco, "Automatic synthesis of fuzzy systems: an evolutionary overview with a genetic programming perspective," *WIREs Data Mining and Knowledge Discovery*, vol. 9, no. 2, Mar. 2018, doi: 10.1002/widm.1251.
- [29] G. Joshi and P. P. A. J., "ANFIS controller for vector control of three phase induction motor," *Indonesian Journal of Electrical Engineering and Computer Science*, vol. 19, no. 3, p. 1177, Sep. 2020, doi: 10.11591/ijeecs.v19.i3.pp1177-1185.
- [30] M. Irshaid and S. Abu-Eisheh, "Application of adaptive neuro-fuzzy inference system in modelling home-based trip generation," *Ain Shams Engineering Journal*, vol. 14, no. 11, p. 102523, Nov. 2023, doi: 10.1016/j.asej.2023.102523.




BIOGRAPHIES OF AUTHORS

Rachida Baz    got in 2014 her License degree in Informatic and Electronics, at the Faculty of Science and Technology Mohammedia affiliated to the University Hassan II at Casablanca-Morocco, then she got a master's degree in biomedical engineering from the Faculty of Science and Technology, Settat, Morocco in 2019. She is currently a Ph.D. student in the Laboratory of Matter, Energy, and System Control (LMECS) at HASSAN II University, Mohammedia-Casablanca, Morocco. Her works, studies, and interests focused on modeling, observation, electric and hybrid vehicle control. She can be contacted at email: rachida.baz@gmail.com.






Khalid El Majdoub    received a Ph.D. degree in automatic control from the Mohammadia School of Engineering in Rabat (Morocco) in 2012. In 2001, he was an Aggregated Professor (*Professeur Agrégé*) in Electrical Engineering from the Ecole Normale Supérieure of Rabat, Morocco. Currently, he is serving as a Professor in Engineering School of electricity and Mechanic ENSEM affiliated to the University Hassan II at Casablanca-Morocco, where he teaches electrical engineering. His main research areas are nonlinear system control and observation, adaptive control, electric vehicle and hybrid electric vehicle control, the Magnetorheological suspension control. He can be contacted at email: k.elmajdoub@ensem.ac.ma.



Fouad Giri    received the Ph.D. degree in automatic control from Institute National Polytechnique de Grenoble, France, in 1988. He is currently Professor at the University de Caen Normandie, France. His research interests include nonlinear system identification, observation and control for finite- and infinite-dimensional systems and application to power electric systems. He has published 6 books and over 120 journal papers. He has served as a Chair of the IFAC TC1.2 and Associate Editor for several journals including automatica, control engineering practice, IEEE transactions on control systems technology. He can be contacted at email: fouad.giri@unicaen.fr.



Ossama Ammari    was born in 1990 in Casablanca, Morocco. In 2016, he was an Aggregated Professor (*Professeur Agrégé*) in the Electrical Engineering from the Centre Régional des Métiers de l'Education et de la Formation Casablanca-Settat, Morocco. He received the Master degree in Electrical Engineering from the Faculty of Science and Technology, University Cadi Ayyad, Marrakech, Morocco, in 2013. The main research areas are nonlinear system control, adaptive control, the electric vehicle and hybrid electric vehicle control. He can be contacted at email: ammari.ossama@gmail.com.